Two-dimensional homogeneous isotropic fluid turbulence with polymer additives

Anupam Gupta,[1,2,*] Prasad Perlekar,[3,†] and Rahul Pandit[1,4,‡]

[1]*Centre for Condensed Matter Theory, Department of Physics, Indian Institute of Science, Bangalore 560012, India*

[2]*Department of Physics, University of Rome "Tor Vergata," Via della Ricerca Scientifica 1, 00133 Roma, Italy*

[3]*TIFR Centre for Interdisciplinary Sciences, 21 Brundavan Colony, Narsingi, Hyderabad 500075, India*

[4]*Jawaharlal Nehru Centre for Advanced Scientific Research, Jakkur, Bangalore, India*

(Received 3 August 2012; revised manuscript received 27 October 2014; published 24 March 2015)

We carry out an extensive and high-resolution direct numerical simulation of homogeneous, isotropic turbulence in two-dimensional fluid films with air-drag-induced friction and with polymer additives. Our study reveals that the polymers (a) reduce the total fluid energy, enstrophy, and palinstrophy; (b) modify the fluid energy spectrum in both inverse- and forward-cascade régimes; (c) reduce small-scale intermittency; (d) suppress regions of high vorticity and strain rate; and (e) stretch in strain-dominated regions. We compare our results with earlier experimental studies and propose new experiments.

DOI: 10.1103/PhysRevE.91.033013 PACS number(s): 47.27.Gs, 47.27.Ak

I. INTRODUCTION

Polymer additives have remarkable effects on turbulent flows: in wall-bounded flows they lead to drag reduction [1,2]; in homogeneous, isotropic turbulence they give rise to dissipation reduction, a modification of the energy spectrum, and a suppression of small-scale structures [3–13]. These effects have been studied principally in three-dimensional (3D) flows; their two-dimensional (2D) analogs have been studied only over the past decade in experiments [14–16] on and direct numerical simulations (DNSs) [17–20] of fluid films with polymer additives. It is important to investigate the differences between 2D and 3D fluid turbulence with polymers because the statistical properties of fluid turbulence in 2D and 3D are qualitatively different [21]: the inviscid, unforced 2D Navier-Stokes (NS) equation admits more conserved quantities than its 3D counterpart; one consequence of this is that, from the forcing scales, there is a flow of energy towards large length scales (an inverse cascade) and of enstrophy towards small scales (a forward cascade). We have, therefore, carried out an extensive and high-resolution DNS study of homogeneous, isotropic turbulence in the incompressible, 2D NS equation with air-drag-induced friction and polymer additives, described by the finitely extensible nonlinear elastic Peterlin (FENE-P) model for the polymer-conformation tensor. We find that the inverse-cascade part of the energy spectrum in 2D fluid turbulence is suppressed by the addition of polymers. We show, for the first time, that the effect of polymers on the forward-cascade part of the fluid energy spectrum in 2D is (a) a slight reduction at intermediate wave numbers and (b) a significant enhancement in the large-wave-number range, as in three dimensions; the high resolution of our simulation is essential for resolving these spectral features unambiguously. In addition, we find dissipation-reduction-type phenomena [7,8]: polymers reduce the total fluid energy and energy- and mean square vorticity- or enstrophy-dissipation rates, suppress small-scale intermittency, and decrease high-intensity vortical and strain-dominated régimes. Our probability distribution functions (PDFs) for σ^2 and ω^2, the squares of the strain rate, and the vorticity, respectively, agree qualitatively with those in experiments [16]. We also present PDFs of the Okubo-Weiss parameter $\Lambda = (\omega^2 - \sigma^2)/8$, whose sign determines whether the flow in a given region is vortical or strain dominated [22,23], and PDFs of the polymer extension; and we show explicitly that polymers stretch preferentially in strain-dominated regions.

The remainder of this paper is organized as follows. In Sec. II we define the equations we use for polymer additives in a fluid and we describe the numerical methods we use to study these equations. Section III is devoted to the results of our study and Sec. IV contains a discussion of our principal results.

II. MODEL AND NUMERICAL METHODS

The 2D incompressible NS and FENE-P equations can be written in terms of the stream function ψ and the vorticity $\boldsymbol{\omega} = \nabla \times \mathbf{u}(\mathbf{x},t)$, where $\mathbf{u} \equiv (-\partial_y\psi, \partial_x\psi)$ is the fluid velocity at point $\mathbf{x}$ and time t, as follows:

$$D_t\omega = \nu\nabla^2\omega + \frac{\mu}{\tau_P}\nabla\times\nabla\cdot[f(r_P)\mathcal{C}] - \alpha\omega + F_\omega; \quad (1)$$

$$\nabla^2\psi = \omega; \quad (2)$$

$$D_t\mathcal{C} = \mathcal{C}\cdot(\nabla\mathbf{u}) + (\nabla\mathbf{u})^T\cdot\mathcal{C} - \frac{f(r_P)\mathcal{C} - \mathcal{I}}{\tau_P}. \quad (3)$$

Here $D_t \equiv \partial_t + \mathbf{u}\cdot\nabla$, the uniform solvent density $\rho = 1$, α is the coefficient of friction, ν the kinematic viscosity of the fluid, μ the viscosity parameter for the solute (FENE-P), and τ_P the polymer relaxation time. To mimic experiments [16], we use a Kolmogorov-type forcing, $F_\omega \equiv k_{\rm inj}F_0\cos(k_{\rm inj}y)$, with amplitude F_0; the energy-injection wave vector is $k_{\rm inj}$ (the length scale $l_{\rm inj} \equiv 2\pi/k_{\rm inj}$); the superscript T denotes a transpose, $\mathcal{C}_{\beta\gamma} \equiv \langle R_\beta R_\gamma\rangle$ are the elements of the polymer-conformation tensor (angular brackets indicate the average over polymer configurations), $\mathcal{I}$ is the identity tensor, $f(r_P) \equiv (L^2-2)/(L^2-r_P^2)$ is the FENE-P potential, and $r_P \equiv \sqrt{\mathrm{Tr}(\mathcal{C})}$ and L are, respectively, the length and the maximal

*agupta@roma2.infn.it

†perlekar@tifrh.res.in

‡rahul@physics.iisc.ernet.in.

TABLE I. Parameters for our DNS runs R1–R10 with the friction coefficient $\alpha = 0.01$. N^2 is the number of collocation points; δt, the time step; $E_{\rm inj}$, the energy-injection rate; ν, the kinematic viscosity; and c, the concentration parameter. The Taylor-microscale Reynolds number is $\mathrm{Re}_\lambda \equiv u_{\rm rms}\lambda/\nu$, where $\lambda = (\int E(k)dk/\int k^2E(k)dk)^{1/2}$ and the Weissenberg number is $\mathcal{W}i \equiv \tau_P\sqrt{\epsilon^f/\nu}$, where ϵ^f is the energy dissipation rate per unit mass for the fluid. The dissipation scale is $\eta_d \equiv (\nu^3/\epsilon)^{1/4}$ and $k_{\rm max} = N/3$.

	N	L	τ_P	$\delta t \times 10^4$	$E_{\rm inj}$	$\nu \times 10^4$	$\mathcal{W}i$	c	Re_λ	$k_{\rm max}\eta_d$
R1	512	6	2	10.0	0.008	10.0	4.71	0.1	107, 85	3.4, 3.6
R2	1024	100	1, 2, 4	1.0	0.005	5.0	2.26, 4.52, 9.04	0.1	221, 121, 53, 38	5.1, 5.3, 5.4, 5.5
R3	2048	100	1	1.0	0.003	5.0	1.81	0.4	147, 60	14.1, 14.8
R4	2048	100	1	1.0	0.0015	5.0	1.35	0.2	86, 54	13.2, 13.6
R5	4096	100	1	1.0	0.005	5.0	2.21	0.2	233, 91	20.2, 20.9
R6	4096	100	1	1.0	0.002	5.0	1.53	0.2, 0.4	108, 62, 45	24.8, 25.8, 26.1
R7	4096	10	1	1.0	0.002	5.0	1.53	0.4	108, 90	24.8, 26.2
R8	4096	100	1	0.5	0.005	1.0	2.91	0.1, 0.4	1451, 1367, 1311	8.0, 8.3, 8.5
R9	4096	10	1	0.5	0.005	1.0	2.91	0.1	1451, 1407	8.0, 8.2
R10	16384	100	1	0.5	0.002	5.0	1.56	0.2	106, 61	96.4, 102.7

possible extension of the polymers; and $c \equiv \mu/(\nu+\mu)$ is a dimensionless measure of the polymer concentration [24].

We use periodic boundary conditions, a square simulation domain with side $\mathbb{L} = 2\pi$ and N^2 collocation points, a fourth-order Runge-Kutta scheme, with time step δt, for time marching, an explicit, fourth-order, central-finite-difference scheme in space, and the Kurganov-Tadmor shock-capturing scheme [25] for the advection term in Eq. (3); the Kurganov-Tadmor scheme (Eq. (7) in Ref. [8]) resolves sharp gradients in $\mathcal{C}_{\beta\gamma}$ and thus minimizes dispersion errors, which increase with L and τ_P. We solve Eq. (2) in Fourier space by using the FFTW library [26]. We choose $\delta t \simeq 10^{-3}$ to 5×10^{-5} so that r_P does not become larger than L (Table I). We preserve the symmetric-positive-definite (SPD) nature of $\mathcal{C}$ by adapting to two dimensions the Cholesky-decomposition scheme from Refs. [7,8,24]: We define $\mathcal{J} \equiv f(r_P)\mathcal{C}$, so Eq. (3) becomes

$$D_t\mathcal{J} = \mathcal{J}\cdot(\nabla\mathbf{u}) + (\nabla\mathbf{u})^T\cdot\mathcal{J} - s(\mathcal{J}-\mathcal{I}) + q\mathcal{J}, \qquad (4)$$

where $s = (L^2-2+j^2)/(\tau_P L^2)$, $q = [d/(L^2-2) - (L^2-2+j^2)(j^2-2)/(\tau_P L^2(L^2-2))]$, $j^2 \equiv \mathrm{Tr}(\mathcal{J})$, and $d = \mathrm{Tr}[\mathcal{J}\cdot(\nabla\mathbf{u}) + (\nabla\mathbf{u})^T\cdot\mathcal{J}]$. Given that $\mathcal{C}$ and hence $\mathcal{J}$ are SPD matrices, we can write $\mathcal{J} = \mathcal{L}\mathcal{L}^T$, where $\mathcal{L}$ is a lower-triangular matrix with elements ℓ_{ij}, such that $\ell_{ij} = 0$ for $j > i$; Eq. (4) now yields ($1 \leqslant i \leqslant 2$ and $\Gamma_{ij} \equiv \partial_i u_j$)

$$\begin{aligned}
D_t\ell_{11} &= \Gamma_{11}\ell_{11} + \Gamma_{21}\ell_{21} + \frac{1}{2}\left[(q-s)\ell_{11} + \frac{s}{\ell_{11}}\right],\\
D_t\ell_{21} &= \Gamma_{12}\ell_{11} + \Gamma_{21}\frac{\ell_{22}^2}{\ell_{11}} + \Gamma_{22}\ell_{21}\\
&\quad + \frac{1}{2}\left[(q-s)\ell_{21} - s\frac{\ell_{21}}{\ell_{11}^2}\right], \qquad (5)\\
D_t\ell_{22} &= -\Gamma_{21}\frac{\ell_{21}\ell_{22}}{\ell_{11}} + \Gamma_{22}\ell_{22}\\
&\quad + \frac{1}{2}\left[(q-s)\ell_{22} - \frac{s}{\ell_{22}}\left(1+\frac{\ell_{21}^2}{\ell_{11}^2}\right)\right].
\end{aligned}$$

Equation (5) preserves the SPD nature of $\mathcal{C}$ if $\ell_{ii} > 0$, which we enforce [7,8] by considering the evolution of $\ln(\ell_{ii})$ instead of ℓ_{ii}.

We have tested explicitly that the statistical properties we measure do not depend on the resolutions we use for our DNS. We check this by both increasing and decreasing this resolution. Indeed, our DNS uses the highest resolution that has been attempted so far for this problem (it uses 256 times as many collocation points as in Ref. [18]). Furthermore, the Kurganov-Tadmor shock-capturing scheme that we use controls any dispersive errors, because of sharp gradients in the polymer-conformation tensor, as in similar 3D studies [7,24].

We maintain a constant energy-injection rate $E_{\rm inj} \equiv \langle\mathbf{F_u}\cdot\mathbf{u}\rangle$ with $F_\omega = \nabla\times\mathbf{F_u}$; the system attains a nonequilibrium, statistically steady state after $\simeq 2\tau_e - 3\tau_e$, where the box-size eddy-turnover time $\tau_e \equiv \mathbb{L}/u_{\rm rms}$ and $u_{\rm rms}$ is the root-mean-square velocity.

In addition to $\boldsymbol{\omega}(\mathbf{x},t)$, $\psi(\mathbf{x},t)$, and $\mathcal{C}(\mathbf{x},t)$ we obtain $\mathbf{u}(\mathbf{x},t)$, the fluid-energy spectrum $E(k) \equiv \sum_{k-1/2<k'\leqslant k+1/2} k'^2\langle|\hat{\psi}(\mathbf{k}',t)|^2\rangle_t$, where $\langle\rangle_t$ indicates the time average over the statistically steady state, the total kinetic energy $\mathcal{E}(t) \equiv \langle\frac{1}{2}|\mathbf{u}(\mathbf{x},t)|^2\rangle_{\mathbf{x}}$, the enstrophy $\Omega(t) \equiv \langle\frac{1}{2}|\boldsymbol{\omega}(\mathbf{x},t)|^2\rangle_{\mathbf{x}}$, and the palinstrophy $\mathcal{P}(t) \equiv \langle\frac{1}{2}|\nabla\times\boldsymbol{\omega}(\mathbf{x},t)|^2\rangle_{\mathbf{x}}$, where $\langle\rangle_{\mathbf{x}}$ denotes the spatial average, the PDF of scaled polymer extensions $P(r_P/L)$, the PDFs of ω^2, σ^2, and $\Lambda = (\omega^2-\sigma^2)/8$, where $\sigma^2 \equiv \sum_{ij}\sigma_{ij}\sigma_{ij}$, and $\sigma_{ij} \equiv \partial_i u_j + \partial_j u_i$, the PDF of the Cartesian components of $\mathbf{u}$, and the joint PDF of Λ and r_P^2. We obtain the isotropic part of the order p, structure function $S_p(r)$ from longitudinal velocity increments as described in Ref. [22]. We concentrate on $S_2(r)$ and the hyperflatness $F_6(r) \equiv S_6(r)/[S_2(r)^3]$; the latter is a measure of the intermittency at the scale r.

III. RESULTS

In Fig. 1(a) we show how $\mathcal{E}(t)$ (top panel), $\Omega(t)$ (middle panel), and $\mathcal{P}(t)$ (bottom panel) fluctuate about their mean values $\langle\mathcal{E}(t)\rangle_t$, $\langle\Omega(t)\rangle_t$, and $\langle\mathcal{P}(t)\rangle_t$ for $c = 0$ (pure fluid) and $c = 0.4$. Clearly, $\langle\mathcal{E}(t)\rangle_t$, $\langle\Omega(t)\rangle_t$, and $\langle\mathcal{P}(t)\rangle_t$ decrease as c increases. Thus, polymers increase the effective viscosity of the solution; but this naïve conclusion has to be refined, as shown later, because the effective viscosity depends on the length scale [6–8].

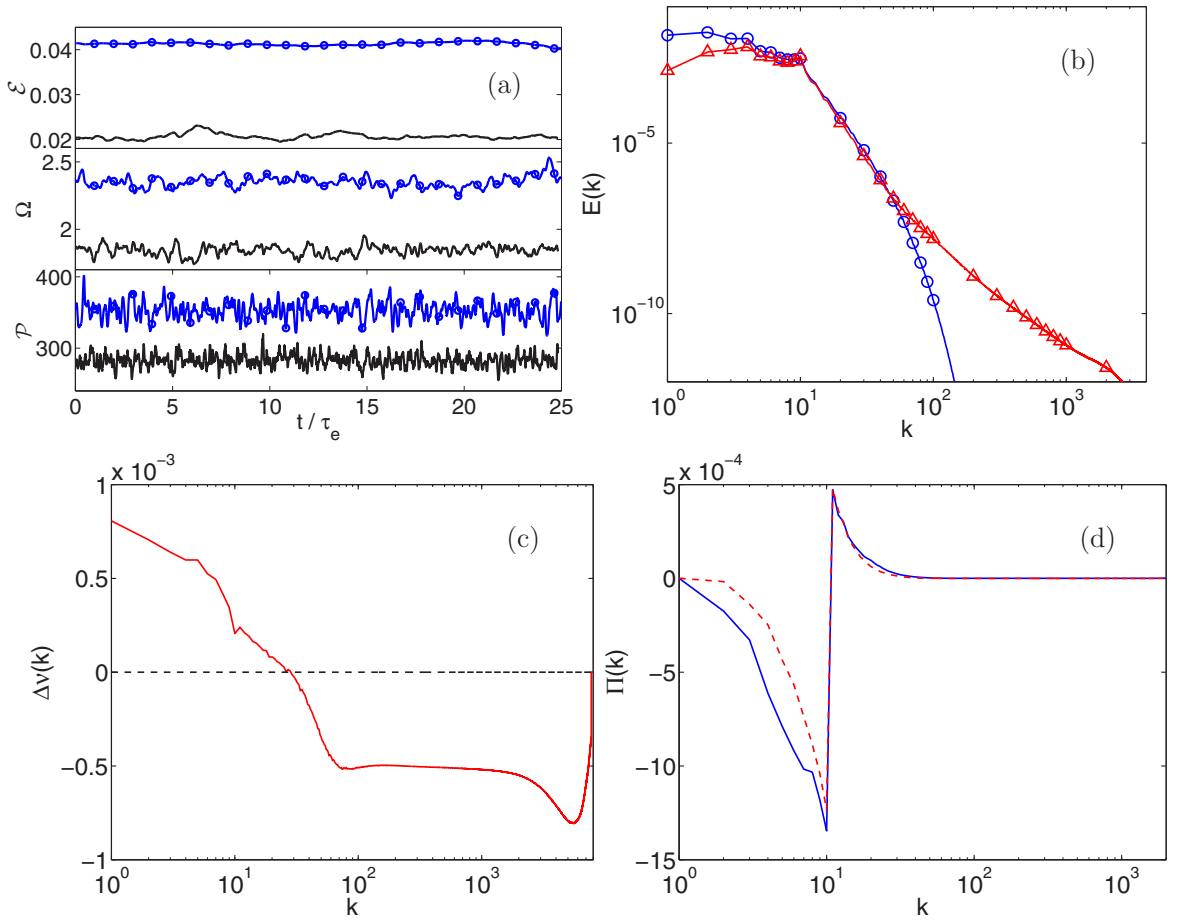

FIG. 1. (Color online) (a) Plots versus time t/τ_e of the total kinetic energy $\mathcal{E}$ of the fluid (top panel), the enstrophy Ω (middle panel), and the palinstrophy $\mathcal{P}$ (bottom panel) for $c = 0$ [upper curve, (blue) circles, run R7] and $c = 0.4$ (lower, black curve, run R7). (b) Log-log (base 10) plots of the energy spectra $E(k)$ versus k for $c = 0.2$ [(red) triangles, run R10] and $c = 0$ [(blue) circles, run R10]. (c) Polymer contribution to the scale-dependent viscosity $\Delta\nu(k)$ versus k for $c = 0.2$ [(red) line, run R10]; $\Delta\nu(k) = 0$ is shown as the dashed black line. (d) Energy flux $\Pi(k)$ versus k for $c = 0.2$ [dashed (red) line, run R10] and $c = 0$ [solid (blue) line, run R10].

In Fig. 2(a), we plot $S_2(r)$ versus r for $c = 0$ [(blue) circles, run R7] and $c = 0.2$ [(green) asterisks, run R7]. The dashed line, with slope 2, is a guide for the eye; this slope agrees with the $S_2(r) \sim r^2$ form that we expect, at small r, by Taylor expansion. At large values of r, $S_2(r)$ deviates from this r^2 behavior, more so for $c = 0.2$ than for $c = 0$, in accord with

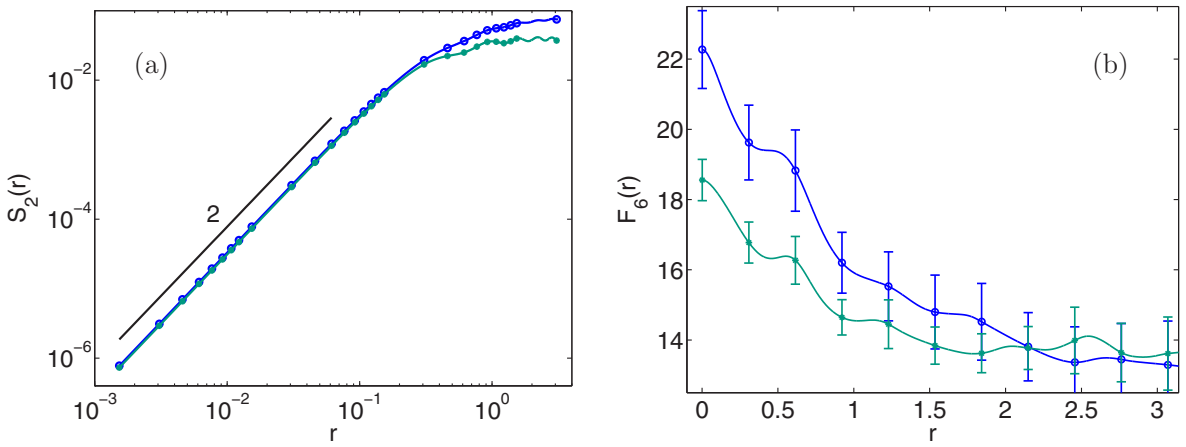

FIG. 2. (Color online) (a) Plots of the second-order velocity structure function $S_2(r)$ versus r for $c = 0$ [(blue) circles, run R7] and $c = 0.2$ [(green) asterisks, run R7]; the line with slope 2 is shown for comparison. (b) Plots of the hyperflatness $F_6(r)$ versus r for $c = 0$ [(blue) circles, run R7] and $c = 0.2$ [(green) asterisks, run R7].

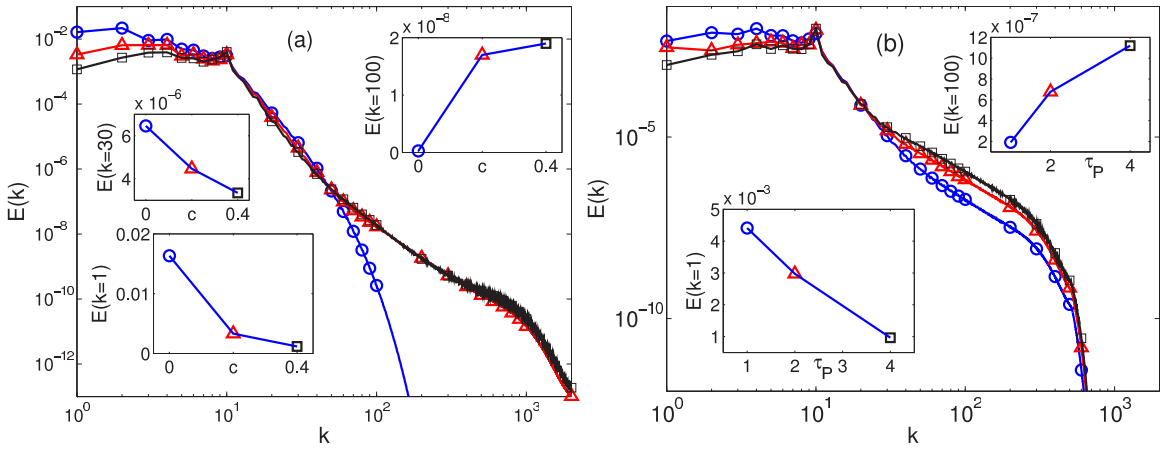

FIG. 3. (Color online) (a) Log-log (base 10) plots of the energy spectra $E(k)$ versus k for $c = 0$ [(blue) circles, run R6], $c = 0.2$ [(red) triangles, run R6], and $c = 0.4$ (black squares, run R6); plots of $E(k)$ versus c for $\mathcal{W}i = 1.53$ and $k = 1$ (bottom-left inset), $\mathcal{W}i = 1.53$ and $k = 30$ (top-left inset), and $\mathcal{W}i = 1.53$ and $k = 100$ (top-right inset). (b) Log-log (base 10) plots of $E(k)$ versus k for $\mathcal{W}i = 2.26$ [(blue) circles, run R2], $\mathcal{W}i = 4.52$ [(red) triangles, run R2], and $\mathcal{W}i = 9.04$ (black squares, run R2); plots of $E(k)$ versus τ_P for $c = 0.4$ and $k = 1$ (bottom-left inset) and $c = 0.4$ and $k = 100$ (top-right inset).

experiments [16]. Plots of $F_6(r)$ versus r [Fig. 2(b)], for $c = 0$ [(blue) circles] and $c = 0.2$ [(green) asterisks, run R8], show that, upon the addition of polymers, small-scale intermittency decreases as c increases.

In Fig. 3(a), we show how $E^p(k)$ changes as we increase c: at low and intermediate values of k (e.g., $k = 1$ and 30, respectively), $E^p(k)$ decreases as c increases, but for large values of k (e.g., $k = 100$), it increases with c. Figure 3(b) shows how $E^p(k)$ changes as we increase τ_P with c held fixed at 0.1. At low values of k (e.g., $k = 1$), $E^p(k)$ decreases as τ_P increases, but for large values of k (e.g., $k = 100$) it increases with τ_P.

In Fig. 4(a) we show plots, for $c = 0.1$, of the spectra $E^p(k)$ for $L = 100$ [(red) triangles, run R8] and $L = 10$ [(green) asterisks, run R9. For comparison we also plot $E^f(k)$ for $c = 0$; as L increases, the difference between $E^p(k)$ and $E^f(k)$ increases at large values of k. We see that the larger the value of L the more pronounced is the rise of the large-k tail of $E^p(k)$ [cf. the plots in Fig. 4(a) with (red) triangles and (green) asterisks for $L = 100$ and $L = 10$, respectively].

We can understand these trends qualitatively by noting that, even at maximal extension, the size of a polymer is $\leqslant \eta$ (the dissipation scale). Thus, the polymers stretch at the expense of the fluid energy, which cascades from intermediate length scales to dissipative scales; this leads to a reduction in $E(k)$ at the values of k that correspond to these intermediate scales. As the polymers relax, they feed energy to the fluid at deep-dissipation, i.e., large-k, scales; this leads to an enhancement of the tail of $E(k)$ at large values of k. The reduction in energy in the inverse-cascade, low-k regime can be understood by noting that polymers enhance the overall, effective viscosity of the fluid. Indeed, in the limit $\tau_P \to 0$, $\nu\nabla^2\mathbf{u} + \frac{\mu}{\tau_P}\nabla \cdot f(r_P)C \to (\nu + \mu)\nabla^2\mathbf{u}$ [27].

To understand quantitatively the effect of polymers on $E(k)$, in different regimes of k, we must compare the fluid-energy spectra with and without polymers [Fig. 1(b)]. This leads

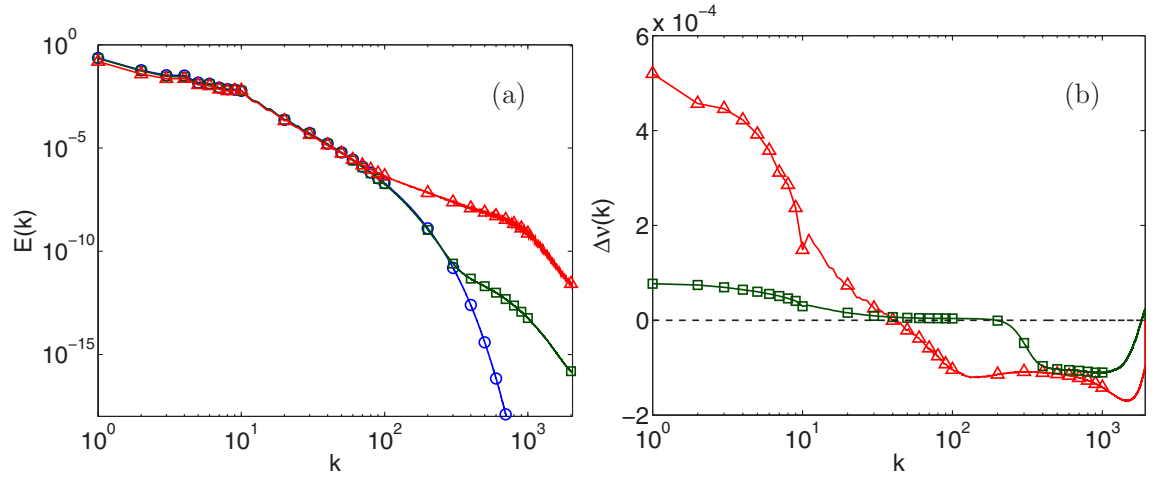

FIG. 4. (Color online) (a) Log-log (base 10) plots, for $c = 0.2$ and $\mathcal{W}i = 2.91$, of $E(k)$ versus k for $L = 100$ [(red) triangles, run R8] and $L = 10$ [(green) asterisks, run R9]; $E(k)$ for $c = 0$ [(blue) circles, run R8]. (b) Plots, for $L = 100$ [(red) triangles, run R8] and $L = 10$ [(green) asterisks, run R9], of the scale-dependent correction to the viscosity $\Delta\nu(k)$ versus k.

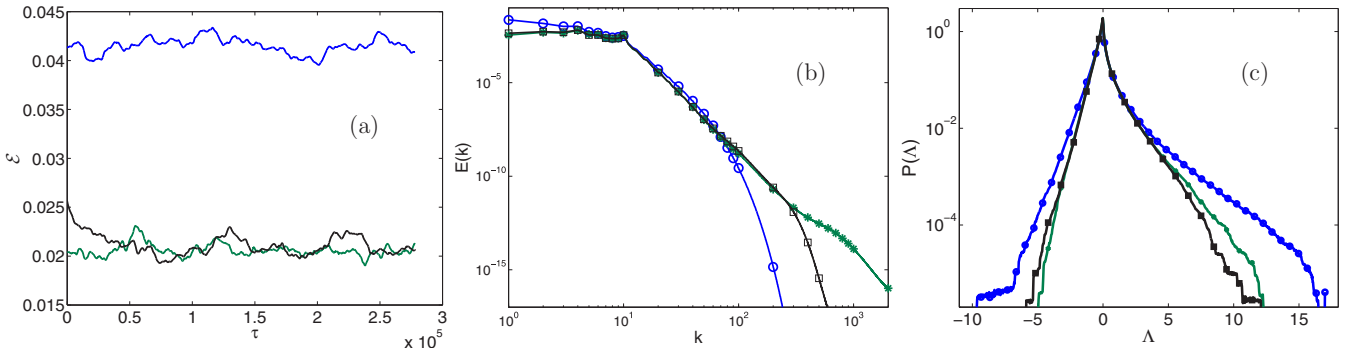

FIG. 5. (Color online) Plots with comparisons of (a) the energy, (b) the energy spectra, and (c) the PDF of Λ from our DNS of the NS equations with the *scale-dependent* viscosity $\nu_e(k)$ (black squares) and from the NS + FENE-P run, R7 [(green) asterisks]. [We calculate $\nu_e(k) \equiv \nu + \Delta\nu(k)$ by substituting our data from run R7 into Eq. (6).] For reference, we also show plots of all these quantities for the NS equation with conventional, *scale-independent* viscosity [(blue) circles].

us naturally to define [6–8] the effective, scale-dependent viscosity $\nu_e(k) \equiv \nu + \Delta\nu(k)$, with

$$\Delta\nu(k) \equiv -\mu \sum_{k-1/2<k'\leqslant k+1/2} \frac{\mathbf{u}_{\mathbf{k}'} \cdot (\nabla \cdot \mathcal{J})_{-\mathbf{k}'}}{[\tau_P k^2 E^p(k)]} \qquad (6)$$

and $(\nabla \cdot \mathcal{J})_{\mathbf{k}}$ the Fourier transform of $\nabla \cdot \mathcal{J}$. Figure 1(c) shows that $\Delta\nu(k) > 0$ for $k < 30$, where $E^p(k) < E^f(k)$, whereas, for large values of k, $\Delta\nu(k) < 0$, where $E^p(k) > E^f(k)$, the superscripts f and p stand, respectively, for the fluid without and with polymers. To understand this dependence on L we plot, in Fig. 4(b), the scale-dependent viscosity $\Delta\nu$ for these two representative values, namely, $L = 100$ [(red) triangles, run R8] and $L = 10$ [(green) asterisks and run R9]. We find that $\Delta\nu$ is positive and higher for $L = 100$, at small values of k, than its counterpart for $L = 10$; this explains why $E^p(k)$ is smaller for $L = 100$ than for $L = 10$ at small k. For large values of k, $\Delta\nu$ is more negative for $L = 100$ than for $L = 10$, so $E^p(k)$ is larger for $L = 100$ than for $L = 10$. Note that $\Delta\nu(k)$ changes its sign, from positive to negative, at a smaller value of k for $L = 100$ than for $L = 10$; therefore, the large-k tail of $E^p(k)$ rises above that of $E^f(k)$ at a smaller value of k for $L = 100$ than for $L = 10$. By using $\nu_e(k)$, which we obtain from our NS + FENE-P run R7, we carry out a DNS of the NS equation, with ν replaced by $\nu_e(k)$. In Fig. 5 we present plots of the energy [Fig. 5(a)], energy spectra [Fig. 5(b)], and PDFs of Λ [Figs. 5(c) and 8], to compare the results of this DNS with those of run R7 (NS + FENE-P); the good agreement of these results shows that the NS equation with the scale-dependent viscosity $\nu_e(k)$ captures the essential effects of polymer additives on fluid turbulence in run R7 (NS + FENE-P). The form of our effective viscosity indicates that, at large length scales, in addition to the friction, polymers also provide a dissipative mechanism. By contrast, at small length scales, polymers inject energy back into the fluid.

Figure 1(d) shows the suppression, by polymer additives, of $\Pi(k) = \int_{k'}^{\infty} T(k')dk'$, where $T(k) = \int \hat{u}_i(-\mathbf{k}) P_{ij}(\mathbf{k}) \widehat{(\mathbf{u} \times \boldsymbol{\omega})}_j(\mathbf{k}) d\Omega$ and $P_{ij}(\mathbf{k}) = \delta_{ij} - \frac{k_i k_j}{k^2}$. The suppression of the spectrum in the small-k régime, which has also been seen in experiments [14] and low-resolution DNS (Fig. 4.12 in Ref. [17]), signifies a reduction of the inverse cascade. The enhancement of the spectrum in the large-k regime leads to the reduction in Ω and $\mathcal{P}$ shown in Fig. 1(a); to identify this enhancement unambiguously requires run R10, which is by far the highest-resolution DNS of Eqs. (1)–(3) (with 256 times more collocation points than in, say, Ref. [18]).

We now plot the PDF $P(r_P/L)$ versus r_P/L in Fig. 6 for $c = 0.1$ and $L = 100$ [(red) triangles, run R8], $c = 0.4$ and $L = 100$ (black squares, run R8), and $c = 0.1$ and $L = 10$ [(green) asterisks, run R9]. The extension of the polymers is bounded between $\sqrt{2} \leqslant r_P \leqslant L$. The lower bound, $r_P = \sqrt{2}$, corresponds to polymers in a coiled state; near the upper bound, with $r_P \sim L$, the polymers are in a stretched state. In Fig. 6, we show that $P(r_P/L)$ shows a distinct, power-law regime, with exponents that depend on c, L, and $\mathcal{W}i$. As $\mathcal{W}i$ increases, this exponent can go from a negative value to a positive value, thus signaling a coil-stretch transition.

In Figs. 7(a)–7(c) we present PDFs of Λ, σ^2, and ω^2, respectively, for $c = 0$ [(blue) circles, run R7] and $c = 0.2$ [(red) triangles, run R7], to show that the addition of polymers

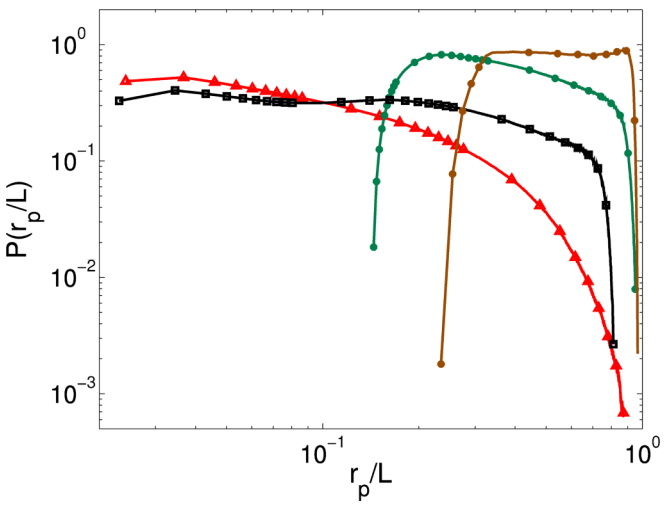

FIG. 6. (Color online) PDFs of the scaled polymer extensions $P(r_P/L)$ versus r_P/L for $c = 0.1$ and $L = 100$ [(red) triangles, run R8], $c = 0.4$ (black squares, run R8), $c = 0.1$ and $L = 10$ [(green) asterisks, run R9], and $c = 0.1$ and $L = 6$ [(brown) circles, run R1].

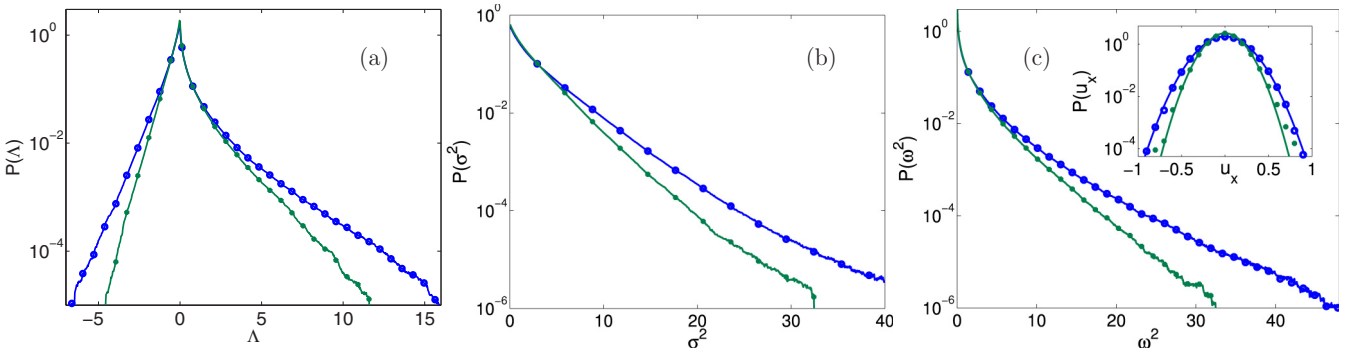

FIG. 7. (Color online) Probability distribution functions (PDFs) of (a) the Okubo-Weiss parameter Λ for run R7, (b) σ^2 for run R7, and (c) ω^2. Inset: PDF of the velocity component u_x for $c = 0$ [(blue) circles, run R7] with a fit $(1/2)\exp(-u_x^2/12.5)$ [solid (blue) line] and for $c = 0.2$ [(green) asterisks, run R7] with a fit $(1/2.65)\exp(-u_x^2/20)$ [solid (green) line]; note that the addition of polymers reduces the rms value of u_x.

suppresses large values of Λ, σ^2, and ω^2. If we make scaled plots of PDFs such as $P(\Lambda/\Lambda_{\rm rms})$, they fall on top of each other for different values of c; this also holds for $P(\sigma^2/\sigma^2_{\rm rms})$ and $P(\omega^2/\omega^2_{\rm rms})$. The inset in Fig. 7(c) shows that the PDF of any Cartesian component of **u** is very close to a Gaussian.

Figure 8(a) shows a conditional PDF of (r_P/L) conditioned on Λ for run R9; this illustrates that polymers stretch predominantly in strain-dominated regions; this is evident very strikingly in Fig. 8(b), which contains a superimposition of contours of r_P^2 on a pseudocolor plot of Λ (for a video sequence of such plots, see [28]).

IV. CONCLUSIONS

We have carried out an extensive and high-resolution DNS of 2D, homogeneous, isotropic fluid turbulence with polymer additives. We have used the incompressible, 2D NS equation with air-drag-induced friction and polymer additives; the latter have been modeled by using the FENE-P model for the polymer-conformation tensor. We find that the inverse-cascade part of the energy spectrum in 2D fluid turbulence is suppressed by the addition of polymers. We demonstrate, for the first time, that the effect of polymers on the forward-cascade part of the fluid energy spectrum in two dimensions is (a) a slight reduction at intermediate wave numbers and (b) a significant enhancement in the large-wave-number range, as in three dimensions; these features are resolved unambiguously by our high-resolution DNS. In addition, we find dissipation-reduction-type phenomena [7,8]: polymers reduce the total fluid energy and energy- and mean-square-vorticity- or enstrophy-dissipation rates. However, as we have emphasized above, dissipation reduction is *not the only notable effect* of polymer additives; our extensive, high-resolution DNS of 2D fluid turbulence with polymer additives yields a good qualitative agreement, in the low-k régime, with the fluid-energy spectra in Ref. [14] and the $S_2(r)$ in Ref. [16]. In addition, our study obtains new results and insights that will, we hope, stimulate new experiments, which should be able to measure (a) the reduction of $\langle\mathcal{E}(t)\rangle_t$, $\langle\Omega(t)\rangle_t$, and $\langle\mathcal{P}(t)\rangle_t$ [Fig. 1(a)]; (b) the modification of $E^p(k)$ at large k [Fig. 1(b)]; (c) the c, τ_P, and L dependences of $E^p(k)$ [Figs. 3(a), 3(b), and 4(a)]; (d) the PDFs of (r_P/L), Λ, σ^2, and ω^2; (e) the stretching of polymers in strain-dominated regions [Fig. 8(b)]; and (f) the suppression of $F_6(r)$ at small r (Fig. 2).

Two-dimensional fluid turbulence with polymer additives has been studied in channel flows, both in experiments [15] and via DNS [20]; this DNS study uses the Oldroyd-B model,

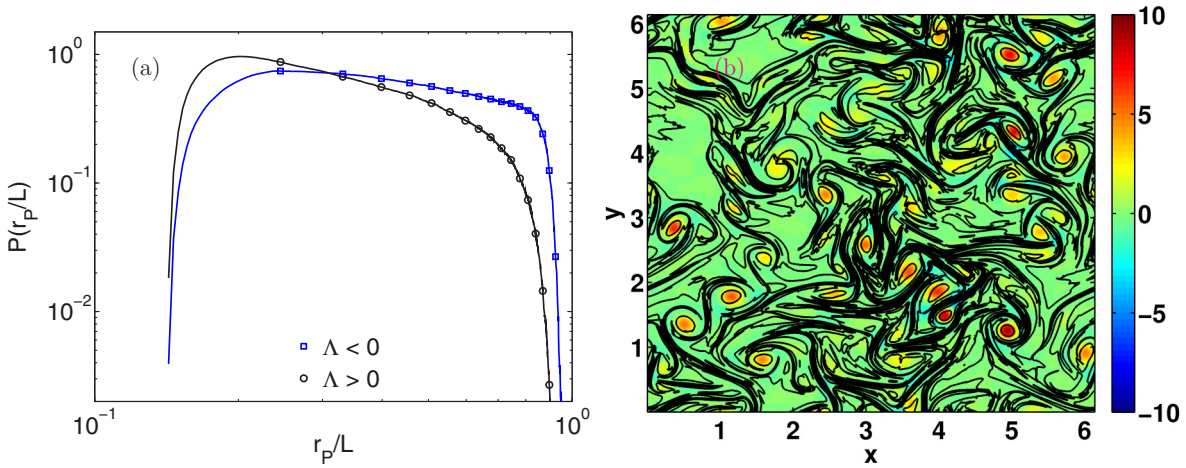

FIG. 8. (Color online) (a) Conditional PDF of (r_P/L) conditioned on Λ for run R9; (b) pseudocolor plot of Λ superimposed on a contour plot of r_P^2 for run R10.

which does not have a maximal polymer extension length and is, therefore, less realistic than the FENE-P model we use. These studies obtain energy spectra and second-order structure functions that are qualitatively similar to those we obtain, except at small length scales, which are not resolved in these channel-flow studies. This shows, therefore, that energy spectra and structure functions, obtained far away from walls, are not affected significantly by the walls. Thus, our studies are relevant to the bulk parts of wall-bounded flows too.

ACKNOWLEDGMENTS

We thank D. Mitra for discussions, Council of Scientific and Industrial Research, University Grants Commission, Department of Science and Technology, and the European Cooperation in Science and Technology Action MP006 for support, and Supercomputing Education and Research Centre (IISc) for computational resources. A.G. is grateful for the grant from the European Research Council under the European Community's Seventh Framework Programme (FP7/2007-2013)/ERC Grant Agreement No. 297004.

[1] B. A. Toms, in *Proceedings of the 1st International Congress on Rheology*, Vol. II (North-Holland, Amsterdam, 1949), p. 135; J. Lumley, J. Polym. Sci. Macromol. Rev. **7**, 263 (1973).
[2] P. Virk, AIChE **21**, 625 (1975).
[3] J. W. Hoyt, Trans. ASME J. Basic Eng. **94**, 258 (1972).
[4] E. van Doorn, C. M. White, and K. R. Sreenivasan, Phys. Fluids **11**, 2387 (1999).
[5] C. Kalelkar, R. Govindarajan, and R. Pandit, Phys. Rev. E **72**, 017301 (2005).
[6] R. Benzi, E. S. C. Ching, and I. Procaccia, Phys. Rev. E **70**, 026304 (2004); R. Benzi, N. Horesh, and I. Procaccia, Europhys. Lett. **68**, 310 (2004).
[7] P. Perlekar, D. Mitra, and R. Pandit, Phys. Rev. Lett. **97**, 264501 (2006).
[8] P. Perlekar, D. Mitra, and R. Pandit, Phys. Rev. E **82**, 066313 (2010).
[9] W.-H. Cai, F.-C. Li, and H.-N. Zhang, J. Fluid Mech. **665**, 334 (2010).
[10] F. De Lillo, G. Boffetta, and S. Musacchio, Phys. Rev. E **85**, 036308 (2012).
[11] N. Ouellette, H. Xu, and E. Bodenschatz, J. Fluid Mech. **629**, 375 (2009).
[12] R. Benzi, E. S. C. Ching, and C. K. Wong, Phys. Rev. E **89**, 053001 (2014).
[13] T. Watanabe and T. Gotoh, Phys. Fluids **26**, 035110 (2014).
[14] Y. Amarouchene and H. Kellay, Phys. Rev. Lett. **89**, 104502 (2002).
[15] H. Kellay, Phys. Rev. E **70**, 036310 (2004).
[16] Y. Jun, J. Zhang, and X.-L. Wu, Phys. Rev. Lett. **96**, 024502 (2006).
[17] S. Musacchio, Ph.D. thesis, Department of Physics, University of Torino, 2003.
[18] S. Berti, A. Bistagnino, G. Boffetta, A. Celani, and S. Musacchio, Phys. Rev. E **77**, 055306(R) (2008).
[19] G. Boffetta, A. Celani, and S. Musacchio, Phys. Rev. Lett. **91**, 034501 (2003); G. Boffetta, A. Celani, and A. Mazzino, Phys. Rev. E **71**, 036307 (2005).
[20] Y. L. Xiong, C. H. Brueneua, and H. Kellay, Europhys. Lett. **95**, 64003 (2011).
[21] G. Boffetta and R. Ecke, Annu. Rev. Fluid Mech. **44**, 427 (2012); R. Pandit, P. Perlekar, and S. S. Ray, Pramana J. Phys. **73**, 157 (2009).
[22] P. Perlekar and R. Pandit, New J. Phys. **11**, 073003 (2009).
[23] A. Okubo, Deep-Sea Res. Oceanogr. Abstr. **17**, 445 (1970); J. Weiss, Physica D (Amsterdam) **48**, 273 (1991).
[24] T. Vaithianathan and L. R. Collins, J. Comput. Phys. **187**, 1 (2003).
[25] A. Kurganov and E. Tadmor, J. Comput. Phys. **160**, 241 (2000).
[26] http://www.fftw.org.
[27] R. B. Bird, C. F. Curtiss, R. C. Armstrong, and O. Hassager, *Dynamics of Polymeric Liquids, Vol. 2: Kinetic Theory*, 2nd ed. (John Wiley, New York, 1987).
[28] See Supplemental Material at http://link.aps.org/supplemental/10.1103/PhysRevE.91.033013 for the video sequence showing pseudocolor plots of the Okubo-Weiss parameter Λ superimposed on contour plots of r_P^2, which measures the polymer extension. Note that polymers stretch predominantly in the strain-dominated regions of the flow.